Hydrol. Earth Syst. Sci. Discuss., 8, 8565–8607, 2011
www.hydrol-earth-syst-sci-discuss.net/8/8565/2011/
doi:10.5194/hessd-8-8565-2011

Hydrology and Earth System Sciences Discussions

Comparing soil moisture retrievals from SMOS and ASCAT over France

M. Parrens[1], E. Zakharova[1], S. Lafont[1], J.-C. Calvet[1], Y. Kerr[2], W. Wagner[3], and J.-P. Wigneron[4]

[1]CNRM-GAME, URA 1357, Météo-France, CNRS, Toulouse, France
[2]CESBIO, UMR 5126, CNES/CNRS/IRD/UPS, Toulouse, France
[3]Institute of Photogrammetry and Remote Sensing, Vienna University of Technology, Vienna, Austria
[4]INRA, EPHYSE, Villenave d'Ornon, France

Received: 9 September 2011 – Accepted: 14 September 2011 – Published: 21 September 2011

Correspondence to: J.-C. Calvet (jean-christophe.calvet@meteo.fr)

Published by Copernicus Publications on behalf of the European Geosciences Union.

Abstract

The first products derived over France in 2010 from the L-band brightness temperatures (T_b) measured by the SMOS (Soil Moisture and Ocean Salinity) satellite, launched in November 2009, were compared with the surface soil moisture (SSM) estimates produced by the C-band Advanced Scatterometter, ASCAT, launched in 2006 on board METOP-A. SMOS and ASCAT SSM products were compared with the simulations of the ISBA-A-gs model and with in situ measurements from the SMOSMANIA network, including 21 stations located in southern France. ASCAT tended to correlate better than SMOS with ISBA-A-gs. The significant anomaly correlation coefficients between in situ observations and the SMOS (ASCAT) product ranged from 0.23 to 0.48 (0.35 to 0.96). However, in wet conditions, similar results between the two satellite products were found. An attempt was made to derive SSM from regressed empirical logarithmic equations using a combination of SMOS T_b at different incidence angles and different polarizations, and the Leaf Area Index (LAI) modeled by ISBA-A-gs. The analysis of the intercept coefficient of the regression showed an impact of topography. A similar analysis applied to ASCAT and SMOS SSM values showed a more limited impact of topography on the intercept coefficient of the SMOS SSM product, while fewer residual geographic patterns were found for the ASCAT SSM.

1 Introduction

Soil moisture plays a key role in the hydrological cycle and in land-atmosphere interactions. For example, evapotranspiration, infiltration and runoff are driven by soil moisture. A number of studies have shown the importance of soil moisture in many applications: atmospheric reanalyses and weather forecast (Beljaars et al., 1996; Frennessy and Shukla, 1999; Diermeyer, 2000), land surface and crop growth modelling (Diermeyer et al., 1999; Georgakakos and Carpenter, 2006; de Wit and van Diepen, 2007; Guerif and Duke, 2000), and hydrometeorology (Eltahir, 1998, among others).

HESSD
8, 8565–8607, 2011

Since the 1970s, remote sensing appears as a potential tool to access soil moisture at different temporal and spatial scales. Indeed, microwave remote sensing is able to provide quantitative information about the water content of a shallow near surface layer (Schmugge, 1983), particularly in the low-frequency microwave range, from 1 to 10 GHz. In the last few years, significant progress towards operational soil moisture monitoring has been made (Wagner et al., 2007).

Passive microwave remote sensing of soil moisture was addressed by many research programs. Various airborne and field campaigns were performed, showing the high potential of L-band (~1.4 GHz) measurements for the estimation of surface parameters (Skou, 1989; Raju et al., 1995; Chanzy et al., 1997; Wigneron et al., 1997; Wilson et al., 2001; Saleh et al., 2004; Calvet et al., 2011; Zribi et al., 2011; Albergel et al., 2011). Moreover, L-band is the optimal wavelength range to observe soil moisture as higher frequencies are more significantly affected by perturbing factors such as atmospheric effects and vegetation cover (Schumugge, 1983; Kerr et al., 2001). Apart from a few days of L-band radiometric observations on Skylab from June 1973 to January 1974 (Eagleman et al., 1976; Jackson et al., 2004), spaceborne microwave radiometers have been operating at frequencies above 5 GHz because the satellite antenna size is directly proportional to the squared wavelength (Ulaby et al., 1982). Recent technological and scientific achievements permitted to develop the Soil Moisture and Ocean Salinity (SMOS) mission (Kerr et al., 2001, 2007) launched in November 2009. SMOS consists of a spaceborne L-band interferometric radiometer able to provide multiangular microwave polarimetric brightness temperatures (T_b), from which a surface soil moisture (SSM) product is derived. Wigneron et al. (1995, 2003) have shown the possibility to retrieve biophysical variables, including SSM, from bipolarized and multiangular microwave T_b. The core component of the SMOS soil moisture retrieval algorithm is the L-band Microwave Emission of the Biosphere (L-MEB) model which simulates the microwave emission at L-band from the soil–vegetation layer (Pellarin et al., 2003b; Wigneron et al., 2007; Kerr, 2010; Panciera et al., 2009). The main difficulty in the estimation of soil moisture using microwave radiometry arises

HESSD
8, 8565–8607, 2011

from the presence of a dense overlying vegetation: the vegetation layer attenuates the soil emission and adds its own emission to the soil emission. Also, the presence of water bodies and of a marked topography may alter the SSM retrieval (Pellarin et al., 2003a, c; Mialon et al., 2008, respectively).

Microwave instruments operating at C-band (close to the L-band), either passive or active, are the Advanced Microwave Scanning Radiometer for the Earth Observing System (AMSR-E on the Aqua satellite), WindSAT (a microwave radiometer on the Coriolis satellite), and the scatterometer on board the European Remote Sensing Satellite (ERS-1, ERS-2). Finally, ASCAT (Advanced Scatterometer) has been orbiting on the METOP meteorological satellite of EUMETSAT since 2006, with a spatial resolution close to SMOS, and C-band radar backscatter measurements at 5.255 GHz (Wagner et al., 2007b; Bartalis et al., 2007a, b). ASCAT was found to accurately reproduce the temporal dynamics of the surface soil moisture measured in situ, or simulated, across different areas in Europe (Albergel et al., 2009, 2010; Brocca et al., 2010b).

Microwave satellite-derived soil moisture products can be retrieved from different microwave remote sensing observations and they need to be verified through in situ soil moisture observations (Rüdiger et al., 2009). Relatively few in situ soil moisture networks are operative now. Since 2006, in southwestern France, the SMOSMANIA (Soil Moisture Observing System, Meteorological Automatic Network Integrated Application) network (Calvet et al., 2007; Albergel et al., 2008) has been measuring soil moisture at different depths. It was extended in 2009 with nine new stations located in southeastern France. As the SMOS products are new, they need to be validated with in situ observations, and compared with other satellite products which have more maturity. Moreover, Albergel et al. (2010) shown that SSM values simulated by the ISBA land surface model (LSM) compare well with the SMOSMANIA in situ observations and with the ASCAT SSM.

In this study, the first SMOS Level 2 product (SMOS-L2 SSM), covering the year 2010, is compared with the SMOSMANIA SSM, together with the ASCAT SSM. The SMOS vs. ASCAT benchmarking is then extended to the whole France domain,

HESSD
8, 8565–8607, 2011

using as a reference a set of SSM simulations performed by a version of the ISBA LSM (ISBA-A-gs) able to simulate SSM, together with the vegetation biomass and Leaf Area Index (LAI), at a spatial resolution of 8 km × 8 km. A simple error model is used to quantify the accuracy of the SMOS SSM products, relative to the ASCAT and ISBA-A-gs data.

Finally, it is shown that the use of the SMOS Level 1 product (SMOS-L1 T_b) permits to investigate the factors affecting the accuracy of the retrieved SSM. Indeed, previous studies have shown that semi-empirical regression equations based on T_b observations can be used to retrieve SSM (Wigneron et al., 2004; Saleh et al., 2006; Calvet et al., 2011). This approach is based on statistical relationships, calibrated from simulated or observed datasets, which require T_b at two distinct incidence angles and/or two polarizations. It was successfully applied to SMOS-L1 data by Albergel et al. (2011). In this study, the SMOS-L1 data are used to estimate SSM based on regression coefficients determined using either SMOSMANIA or the ISBA-A-gs SSM for the year 2010.

The various data sets used in this study are presented in Sect. 2, together with the statistical methods used to analyze the data. Section 3 presents the results and Sect. 4 summarizes a discussion of the main findings. Finally, the main conclusions are presented in Sect. 5.

2 Material and methods

2.1 Satellite data

In this study, the L1 and L2 SMOS products (T_b and SSM, respectively) are investigated for the year 2010, together with the ASCAT SSM.

2.1.1 The SMOS products

The SMOS mission is a joint program of the European Space Agency (ESA), the Centre National d'Etudes Spatiales (CNES), and the Centro para el Desarrollo Tecnológico

HESSD
8, 8565–8607, 2011

Industrial (CDTI), in the framework of the Earth Explorer Opportunity Mission initiative. Over land, the aim of SMOS is to provide global SSM maps with an accuracy better than 0.04 $m^3 m^{-3}$, a spatial resolution better than 50 km, every three days. Also, the vegetation water content can be estimated with an accuracy of 0.5 $kg m^{-2}$ every six days (Kerr et al., 2001). The SMOS instrument is a L-band (21 cm, 1.42 GHz) 2-D interferometric radiometer. At L-band, the atmospheric contribution to the signal is limited, and clouds and atmospheric water content have negligible effects (Kerr and al., 1993). Moreover, L-band is more sensitive to soil moisture than higher frequencies over vegetated areas (Schmugge, 1998; Wigneron et al., 1995; Calvet et al., 2011).

SMOS has a sun-synchronous orbit at 757 km altitude (±1 km) with a 06:00 Local Standard Time (LST) ±15 min ascending equator crossing time. This time was chosen in order to minimize factors impacting soil moisture retrieval, such as vertical soil-vegetation temperature gradients, and the Faraday rotation in the ionosphere. A two-dimensional picture is generated by SMOS every 2.4 s. The average ground resolution is 43 km and the globe is fully imaged every three days at 06:00 and 18:00 LST. The radiometric sensitivity of SMOS radiometer over land is 3.5 K per snapshot at boresight (McMullan et al., 2009). The SMOS instrument measures the cross correlations between pairs of receivers to derive a visibility function. In a first approximation, the L-band T_b of the source is computed as the inverse Fourier transform of this function (McMullan et al., 2009). Finally, T_b is measured at several incidence angles, for two polarizations. It is important to note that the SMOS signal can be perturbed by man-made Radio Frequency Interferences (RFI) that degrade the scientific retrievals. Indeed, radio signals received in the L-band are sensitive to RFI (Njoku et al., 2005). Asia and Europe are particularly affected by this phenomenon (Oliva et al., 2011). In Europe, France is not the most affected country. However, Albergel et al. (2011) had to filter out about half of airborne T_b observations affected by RFI, over 11 sites in southwestern France. Two types of RFI were identified by Pardé et al. (2011) in southwestern France: pulsed RFI (due to radars, air traffic control or military installations) and continuous-wave RFI. The latter can trigger very high values of T_b.

HESSD
8, 8565–8607, 2011

In this study, reprocessed data for the year 2010 were used. In a first stage, the SMOS-L1 T_b product was projected from the antenna (X, Y polarizations) to the Earth surface (H and V polarizations) reference frame. The T_{bX} and T_{bY} values were transformed into T_{bH} and T_{bV} values and corrected for Faraday rotation using an algorithm provided by the CESBIO team (http://www.cesbio.ups-tlse.fr/SMOS_blog/wp-content/uploads/TOOLS/XY2HV.m). In order to remove the data contaminated by the most intense RFI, a filtering procedure was applied to the T_b. First, all the T_{bH} and T_{bV} measurements were filtered for extreme values exceeding the median $T_b \pm 50$ K, for each grid point at a given date. Second, we applied a locally weighted scatterplot smoothing technique, known as LOESS, or LOWESS filtering. It is based on fitting by a simple model the localized data subsets (Cleveland and Devil, 1988) in a predefined window. A window of 2.5° was employed as it captured well most of the T_b aberrations caused by RFI. Third, bipolarized values of T_b were extracted for incidence angles (θ) of 20°, 30°, 40° and 50°. For each value of θ, a median T_b was calculated in the range of $\theta \pm 2$°. Then, RFI perturbations were further filtered out. The RFI filtering criterion was based on halved first Stokes parameter calculated as $T_bS1 = 0.5(T_{bH} + T_{bV})$ (Kerr et al., 2007). The mean values of T_bS1 were calculated for the full year 2010 over the France domain, and the T_b measurements out of a two standard deviation interval were considered to be contaminated by RFI. In spite of this processing, residual low RFI perturbations may remain in the data set.

The SMOS-L2 (SSM) product was extracted over the France domain. The L2 algorithm is complex and uses the polarization and multi-angular information delivered by SMOS. It involves direct model inversions and decision trees, and uses ancillary data such as air temperature, soil texture and land cover information.

In 2010, numerous technical and algorithm corrections were performed and affected both L1 and L2 products. In this study, new reprocessed L1 and L2 data, based on the same algorithm, were used. As recommended by Jackson (1980), only the ascending passes (between 04:00 and 07:00 LST over France) were used, because the soil is most likely to be in hydraulic near-equilibrium.

HESSD
8, 8565–8607, 2011

2.1.2 The ASCAT soil moisture product

ASCAT is a real aperture radar measuring radar backscatter with a very good radiometric accuracy and stability (Bartalis et al., 2007b). ASCAT uses VV polarization at C-band. METOP has a sun-synchronous orbit, with equator crossing times of approximately 21:30 LST for the ascending overpass and 09:30 LST for the descending overpass. ASCAT observes 82 % of the globe each day at a spatial resolution of 25–35 km (resampled to a 12.5 km grid). Measurements are performed on both sides of the satellite track, and two 550 km wide swaths of data are produced. This results in three independent backscatter measurements at different viewing angles and separated by a short time delay (Attema, 1991). In order to retrieve SSM, the backscattering coefficients are extrapolated to a reference angle at 40°, and scaled between the lowest and highest values measured over a long period (Wagner et al., 1999a, b, c). Using such a change detection approach, the obtained SSM value represents the degree of saturation of the topmost soil layer (0.5 cm to 2 cm), reported in percentage unit. This value is scaled between 0 % (the minimum soil moisture) and 100 % (the maximum soil moisture).

In this study, an updated ASCAT SSM dataset supplied by Vienna University of Technology (TU-Wien), resampled on a 12.5 km grid, was used. As for SMOS, only morning passes (between 08:00 and 11:00 LST over France) were considered.

2.2 The SMOSMANIA network

The main objective of the SMOSMANIA network is to verify remotely sensed and modeled soil moisture products. This network was designed to validate the SMOS SSM estimates (Calvet et al., 2007). SMOSMANIA is based on the existing automatic weather station network of Météo-France. Twenty-one stations were equipped with four soil moisture probes (ThetaProbe ML2X of Delta-T Devices), horizontally installed at depths of 5, 10, 20 and 30 cm, performing measurements at regular intervals of 12 min. The SMOSMANIA SSM data are in units of $m^3\,m^{-3}$.

HESSD
8, 8565–8607, 2011

Twelve stations were installed in 2006 in southwestern France, following a Mediterranean-Atlantic transect (Albergel et al., 2008). In 2008, the network was extended, with nine new stations located in the Mediterranean region (Fig. 1). Most of the stations are at low altitude and on reasonably flat terrains, with the exception of Barnas, La-Grand-Combe, Mouthoumet, Berzème, and Mazan-Abbaye (BRN, LGC, MTM, BRZ, and MZN, respectively) at 480 m, 499 m, 538 m, 650 m, and 1240 m above sea level, respectively. During the installation of soil moisture probes, soil samples were collected at the four depths of the soil moisture profile in order to calibrate the probe. The soil characteristics of the new stations, listed from East to West, are presented in Table 1.

Consistent with the SMOS morning passes used in this study, SMOSMANIA observations at a depth of 5 cm, between 04:00 UTC and 07:00 UTC were used. For ASCAT, observations between 08:00 UTC and 11:00 UTC were used. For both SMOS and ASCAT, daily average SMOSMANIA morning SSM values were computed.

2.3 The ISBA-A-gs LSM

In the ISBA (Interactions between Surface, Biosphere, and Atmosphere, Noilhan and Planton, 1989; Noilhan and Mahfouf, 1996) LSM used in this study, the soil hydrology is based on the force restore approach, according to Deardorff (1978). The root-zone is represented by one bulk reservoir corresponding to the maximum rooting depth, including a skin surface layer (~1 cm thick). Also, a deeper soil layer is represented (Boone et al., 1999), and an explicit multilayer snow model is used (Boone and Etchevers, 2001). The soil and vegetation parameters used by ISBA are derived from a global database of soils and ecosystems, ECOCLIMAP (Masson et al., 2003). In this study, a new version of the ECOCLIMAP dataset (Faroux et al., 2009) was used. It contains an updated classification of vegetation types over Europe and North Africa. Moreover, the ISBA-A-gs (Calvet et al., 1998) version of the LSM was used. It is able to simulate the diurnal cycle of carbon and water vapour fluxes, together with LAI and soil moisture. ISBA-A-gs was used "offline", i.e. without coupling the LSM with an atmospheric model.

HESSD
8, 8565–8607, 2011

The atmospheric forcing was produced by SAFRAN (Système d'Analyse Fournissant des Renseignements Atmosphérique à la Neige, Durant et al., 1993) and the LSM was used at a spatial resolution of 8 km × 8 km to produce daily estimates of SSM and soil temperature at 07:00 UTC, and of LAI.

2.4 Data preparation

2.4.1 Soil moisture products

In order to compare ASCAT, SMOS and ISBA-A-gs SSM values, the satellite products were projected to the ISBA-A-gs 0.070° resolution (8 km × 8 km) grid. The original resampled SMOS and ASCAT grids are 0.146° × 0.135° and 0.125° × 0.125°, respectively. The projection was made by assigning each SMOS (ASCAT) data to all the ISBA-A-gs grid cells within 0.18° (0.15°) using a nearest neighbor approach (Draper et al., 2011a). Before the SMOS data were projected on the ISBA-A-gs grid, observations with a data quality index greater than 30 % were removed. Similarly, ASCAT values with an estimated soil moisture error greater than 30 % were removed. For all the dates with ASCAT observations flagged as frozen soil, flooded surfaces or covered by snow, no ASCAT-SMOS comparison was performed. Moreover, for SMOS-L2 and ASCAT products, a static mask was applied to remove (i) urban regions, identified as having an urban fraction greater than 15 % in the ECOCLIMAP database (ii) steep mountainous terrain, identified as having a topographic complexity flag provided with the ASCAT data greater than 15 %. Finally, in order to remove all the observations corresponding to soil freezing soil conditions, an additional filter was applied to all the products: all the observations corresponding to SAFRAN air temperatures smaller than 277 K were removed.

In order to better capture the day to day variability of SSM, the seasonal cycle was removed by calculating monthly SSM anomalies (Albergel et al., 2009). The difference to the mean was calculated for a sliding window of five weeks (if there were at least five measurements during this period), and the difference was scaled to the standard

HESSD
8, 8565–8607, 2011

deviation. For each soil moisture SSM estimate at day (i), a period F was defined, with $F=[i-17d,\ i+17d]$ corresponding to a five week window. The anomaly Θ is dimensionless and it is given by:

$$\Theta(i) = \frac{\mathrm{SSM}(i) - \overline{\mathrm{SSM}(F)}}{\mathrm{Stdev}(\mathrm{SSM}(F))} \quad (1)$$

This equation was used to compute SSM anomalies from ASCAT, SMOS, ISBA-A-gs, and in-situ observations.

2.4.2 Analysis of the SMOS-L1 T_b data

For SMOS-L1, the same static mask applied for SMOS-L2 and ASCAT (see Sect. 2.4.1) was used. In addition to the RFI filtering procedure described in Sect. 2.1.1, the dynamic SMOS-L2 flag was applied to SMOS-L1. As SSM values are considered in this study, the SMOS-L1 T_b were transformed into SSM values, using a simple regression technique based on semi-empirical statistical relationships between reference SSM values and T_b values at two contrasting incidence angles and/or two polarizations (Wigneron et al., 2004; Saleh et al., 2006b; Calvet et al., 2011; Albergel et al., 2011). Mattar et al. (2011) shown that an additional information on the vegetation development (such as the Normalized Difference Vegetation Index (NDVI), or the LAI) can improve the regression. In this study, a regression equation based on two incidence angles (θ_1 and θ_2), two polarizations (p and q) and LAI estimates was used (adapted from Mattar et al., 2011):

$$\mathrm{SSM} = \exp\left(A\ln\left(1-\frac{T_b(\theta_1,p)}{T_{\mathrm{eff}}}\right) + B\ln\left(1-\frac{T_b(\theta_1,q)}{T_{\mathrm{eff}}}\right) + C\ln\left(1-\frac{T_b(\theta_2,p)}{T_{\mathrm{eff}}}\right) + D\ln\left(1-\frac{T_b(\theta_2,q)}{T_{\mathrm{eff}}}\right) + E\,\mathrm{LAI} + F\right) \quad (2)$$

In Eq. (2), the LAI and the SSM are derived from reference ISBA-A-gs LSM simulations or, in the case of SSM, from SMOSMANIA SSM observations. The T_{eff} values

HESSD
8, 8565–8607, 2011

were derived from the surface temperature computed by ISBA-A-gs. The regression coefficients A, B, C, D, E and F vary from one grid cell to another and depend on surface characteristics (Saleh et al., 2006).

Also, a regression analysis was applied to the SMOS-L2 SSM:

$$\mathrm{SSM} = A' \, \mathrm{SSM}_{\mathrm{SMOS}} + B' \tag{3}$$

and to ASCAT data:

$$\mathrm{SSM} = A^* \, \mathrm{SSM}_{\mathrm{ASCAT}} + B^* \tag{4}$$

In Eqs. (3) and (4), the reference SSM values were derived from ISBA-A-gs LSM simulations. In Eq. (4) the SSM simulated by ISBA-A-gs was rescaled between field capacity and wilting point values in order to be consistent with the ASCAT SSM. As for SMOS-L1 T_b in Eq. (2), the regression coefficients A', B', and A^* and B^* of Eqs. (3) and (4), respectively, vary from one grid-cell to another.

2.4.3 Subset score analysis

Separate analyses were performed for contrasting vegetation and soil moisture conditions, for the three main surface types in France: crops, forests (either broadleaf or coniferous) and grasslands. A 8 km × 8 km grid cell was considered as representative of a given vegetation type (either crops, forests or grasslands), when the fraction of this vegetation type given by the ECOCLIMAP database was greater than 50 %. The LAI variable was chosen to characterize vegetation conditions. In the ISBA-A-gs simulations used in this study, the median LAI value was 1.66 $\mathrm{m^2\,m^{-2}}$. Under (over) this value, the vegetation was considered as sparse (dense). The root-zone soil moisture was used to distinguish dry from wet soil conditions. In order to account for the different soil types represented by ISBA-A-gs, the root-zone soil moisture ($\mathrm{m^3\,m^{-3}}$) was converted into dimensionless units by scaling by the soil moisture at saturation. The resulting scaled soil moisture ranged between 0 and 1. The median value of the

HESSD
8, 8565–8607, 2011

simulated normalized root-zone soil moisture was 0.60. Under (over) this value the soil was considered as dry (wet).

2.5 Triple collocation method

A triple collocation error analysis was used to assess the relative error of the SSM products from active (ASCAT) and passive (SMOS) microwave sensors and from the ISBA-A-gs simulations. The triple collocation is a powerful statistical tool to estimate the RMSE while simultaneously solving for systematic differences in the climatologies of a set of three linearly related data sources with independent error structures (Scipal et al., 2008b; Dorigo et al., 2010). This method was recently introduced by Scipal et al. (2008b) in the field of satellite-based soil moisture research. It is assumed that three estimates Θ_{ASCAT} (ASCAT SSM anomaly), Θ_{SMOS} (SMOS SSM anomaly) and Θ_{ISBA} (SSM anomaly calculated by ISBA-A-gs) relate to hypothetical true soil moisture anomaly Θ in a linear fashion (Stoffelen, 1998):

$$\begin{aligned} \Theta_{ASCAT} &= \Theta + \alpha_{ASCAT} + \varepsilon_{ASCAT} \\ \Theta_{SMOS} &= \Theta + \alpha_{SMOS} + \varepsilon_{SMOS} \\ \Theta_{ISBA} &= \Theta + \alpha_{ISBA} + \varepsilon_{ISBA} \end{aligned} \quad (5)$$

Where ε_{ASCAT}, ε_{SMOS} and ε_{ISBA} denote the residual errors in the estimates of Θ_{ASCAT}, Θ_{SMOS}, and Θ_{ISBA}, and α_{ASCAT}, α_{SMOS} and α_{ISBA} represent the calibration constants. In order to eliminate the calibration constants, new variables $\Theta'_X = \Theta_X - \alpha_x$ are introduced (with subscript X standing for ASCAT, SMOS and ISBA respectively). Since scaled anomalies are used (Eq. 1), the standard deviations of the three data sets are similar, suggesting that this additive error model is a reasonable approximation rather than an error model including a multiplicative component such as that used by Scipal et al. (2008). As the three soil moisture estimates used here are entirely independent, it can be assumed that their random errors are uncorrelated, and a direct estimate of the

HESSD
8, 8565–8607, 2011

variance of residual errors is obtained:

$$\begin{aligned} \mathrm{VAR}(\varepsilon_{\mathrm{ASCAT}}) &= (\Theta'_{\mathrm{ASCAT}} - \Theta'_{\mathrm{SMOS}})(\Theta'_{\mathrm{ASCAT}} - \Theta'_{\mathrm{ISBA}}) \\ \mathrm{VAR}(\varepsilon_{\mathrm{SMOS}}) &= (\Theta'_{\mathrm{ASCAT}} - \Theta'_{\mathrm{SMOS}})(\Theta'_{\mathrm{SMOS}} - \Theta'_{\mathrm{ISBA}}) \\ \mathrm{VAR}(\varepsilon_{\mathrm{ISBA}}) &= (\Theta'_{\mathrm{ASCAT}} - \Theta'_{\mathrm{ISBA}})(\Theta'_{\mathrm{ASCAT}} - \Theta'_{\mathrm{ISBA}}) \end{aligned} \quad (6)$$

In 2010, the maximum number of SMOS-ASCAT-ISBA-A-gs triplets was 72, and the grid-cells located in southwestern France presented the highest triplet numbers. In the triple collocation study, only the grid-cells in southwestern France, with at least 40 triplets were considered.

3 Results

3.1 Comparison between SMOS and ASCAT SSM products

SMOS and ASCAT SSM products were evaluated using the SMOSMANIA in situ observations in southern France, and the ISBA-A-gs SSM simulations over the whole of France, for the year 2010.

3.1.1 Comparison at the SMOSMANIA stations in southern France

Statistical scores for the comparison between SMOS and ASCAT SSM anomalies and in situ SSM anomalies were determined. As described in Sect. 2.4.1, the satellite data were projected onto the ISBA-A-gs grid, and the SMOS and ASCAT time series for each SMOSMANIA site were taken from the corresponding ISBA-A-gs grid cell. Albergel et al. (2011) assessed the consistency between SMOS-L1 data, airborne L-band radiometry observations, and the SMOSMANIA in situ observations at 11 stations. They found a good agreement of SMOS-L1 data with the other data sets for 9 of the 11 stations. In particular, very good results were obtained for the Montaut (MNT)

HESSD
8, 8565–8607, 2011

station. Figure 2 presents anomaly time series from in situ measurements, SMOS SSM and ASCAT SSM at the MNT station for 2010. Most peaks and troughs are represented well. The SSM anomaly statistical scores are presented in Table 2 for SMOS ascending orbits and for ASCAT descending orbits. While significant correlations (r_{ano}) are found for 20 stations for ASCAT, 17 stations show significant r_{ano} values for SMOS. For the stations showing significant SSM r_{ano} values, the SMOS (ASCAT) r_{ano} range from 0.23 to 0.60 (0.35 to 0.96), with an average value of 0.36 (0.55). For both SMOS and ASCAT, the highest r_{ano} between satellite SSM anomalies and in situ SSM anomalies, are observed for the Lézignan-Corbières (LZC) station. However, for this station, 2010 measurements are available from January to March and in November, only. These months correspond to wet periods including many rain events triggering marked SSM changes, and this can explain the better correlation.

The SMOS and ASCAT RMSE values range from 0.83 to 1.25, and from 0.33 to 1.07, respectively, with average values of 1.05 and 0.86, respectively, in units of standard deviation. Finally, the SMOS and ASCAT biases range from −0.15 to 0.19, and from −0.11 to 0.11, respectively, with average values of 0.03 and −0.03, respectively. For the stations associated to significant correlations, no systematic dry or wet SSM anomaly bias is observed.

For ASCAT, the MTM station, only, presents non-significant r_{ano} values. MTM is situated close to a forested and mountainous area, and its location can explain the poor results. The SMOS SSM seems to be more affected by topography than ASCAT, as non-significant results are found for five stations (Sabres (SBR), MTM, LGC, MZN and BRN), three of which (MZN, BRN, and MTM) present among the highest altitudes of the SMOSMANIA stations (1165 m, 672 m, and 499 m, respectively).

Regarding absolute correlation (r_{abs} in Table 2), two stations (SBR and BRN) present non-significant r_{abs} values for SMOS, one for ASCAT (MTM). For the stations showing significant SSM r_{abs} values, the SMOS (ASCAT) r_{abs} range from 0.34 to 0.61 (0.19 to 0.82), with an average value of 0.49 (0.64). For SMOS and ASCAT, the highest r_{abs} is observed for Urgons (URG) and SBR, respectively. Overall, r_{abs} values are

HESSD
8, 8565–8607, 2011

higher than r_{ano} values. Indeed, the absolute correlation is explained to a large extent by seasonal variations, which are suppressed in SSM anomalies. In particular, non-significant SMOS-L2 r_{ano} values are observed for MTM and LGC, while they present significant r_{abs} values.

Figure 3 presents SMOS-L2 vs. ASCAT SSM absolute and anomaly correlation coefficients with the in situ observations, for the 21 SMOSMANIA stations. In general, the ASCAT SSM correlates better than the SMOS SSM with the in situ observations. Four stations present better significant r_{abs} values for SMOS-L2: Prades-le-Lez (PRD), MZN, Villevieille (VLV), and Cabrières d'Avignon (CBR). On the other hand, only one station (MZN) present better significant r_{ano} values for SMOS-L2.

3.1.2 Comparison over France using SSM values simulated by ISBA-A-gs

Simulations of SSM values by the ISBA-A-gs LSM were used to generalize the SMOS vs. ASCAT benchmarking results found at the SMOSMANIA stations to other locations in France. In order to compare the satellite products with ISBA-A-gs, statistical scores were calculated for each grid cell of the ISBA-A-gs simulations. Figure 4 shows maps of anomaly correlation, RMSE and p-value between the SMOS and ASCAT SSM and the SSM calculated by ISBA-A-gs over France for the year 2010. In these maps, only significant values are plotted (p-value < 0.05). The significant anomaly correlations range from $r_{ano} = 0.24$ to 0.69 for SMOS and from $r_{ano} = 0.24$ to 0.85 for ASCAT. On average, ASCAT presents better anomaly scores than SMOS, with average values of r_{ano}, RMSE and mean bias of 0.65, 0.78, and −0.01, respectively, against 0.40, 1.04, and 0.07, respectively, for SMOS.

Figure 5 presents SMOS vs. ASCAT SSM anomaly correlation coefficients with the ISBA-A-gs simulations, for the France domain. Only significant correlations (p-value < 0.05) are shown. For the majority of the grid cells, correlation coefficients are greater for ASCAT than for SMOS. The ISBA-A-gs grid cells corresponding to the SMOSMANIA stations are indicated, and more marked differences than those shown by Fig. 3 using SMOSMANIA data are found, with systematically higher ASCAT r_{ano}

HESSD
8, 8565–8607, 2011

values. In Fig. 5, the r_{ano} values are calculated for the whole 2010 year. In order to investigate possible seasonal changes in the relative consistency of SMOS and ASCAT with ISBA-A-gs, the r_{ano} values were disaggregated following the subset analysis described in Sect. 2.4.3.

Figure 6 shows the SMOS vs. ASCAT SSM anomaly correlation coefficients with the ISBA-A-gs simulations, disaggregated in four vegetation and soil wetness classes, for each dominant cover type. Consistent with Fig. 5, ASCAT tends to outperform SMOS, but less systematically. Among the twelve sub-figures of Fig. 6, five present more than 40 % of scores better for SMOS than for ASCAT. These cases correspond to forests (either sparse or dense) in wet conditions, sparse crops in wet conditions, sparse grasslands in dry conditions, and dense grasslands in wet conditions. Except for sparse grasslands and dense crops, SMOS tends to perform as well as ASCAT, in wet conditions. On the other hand, better agreement with ISBA-A-gs SSM simulations is generally achieved by ASCAT in dry conditions.

3.1.3 Relative error estimation over southwestern France

Figure 7 shows the errors derived from the triple collocation analysis of the SSM anomalies of ASCAT, SMOS, and ISBA-A-gs for the year 2010 over southwestern France. The sqrt(VAR(ε_X)) errors, i.e. the square root of the value obtained from Eq. (6), are expressed in units of $m^3\,m^{-3}$, based on the dynamic range of the ISBA-A-gs soil moisture data. The results of the error estimation suggest that all three datasets are characterized by a lower error than the raw estimates given in Sect. 3.1.2. The mean global errors for ISBA-A-gs, SMOS and ASCAT, are $0.022\,m^3\,m^{-3}$, $0.045\,m^3\,m^{-3}$, and $0.031\,m^3\,m^{-3}$, respectively. The average errors found in this study are close to those obtained by Scipal et al. (2008b) at a global scale for a combination of the SSM estimates derived from ERA-Interim, the TMI radiometer, and the ERS-2 scatterometer: $0.020\,m^3\,m^{-3}$, $0.046\,m^3\,m^{-3}$, and $0.028\,m^3\,m^{-3}$, respectively. The spatial patterns of the errors shown by Fig. 7 show that SMOS-L2 presents more relative errors close to

HESSD
8, 8565–8607, 2011

mountainous areas (Pyrenees and Massif Central), as well as over the Les Landes forest (in the area around 0.5° E, 44° N).

3.2 Soil moisture estimates derived from the SMOS T_b

3.2.1 At the SMOSMANIA stations in southern France

In this section, the Eq. (2) empirical relationship is used to estimate SSM from SMOS-L1 data, using the SMOSMANIA in situ data as a reference for the determination of the correlation coefficients. The LAI values used in Eq. (2) are given by the average LAI simulated by ISBA-A-gs for the corresponding grid-cell. Table 3 presents the SSM estimate scores obtained using SMOS T_b values at incidence angles of 40° and 20°. This particular biangular configuration presents the best score. For the LZC station in 2010, in situ SSM observations are available only from January to Mars and in November, and this station was not used. The SSM estimates derived from Eq. (2) are significantly correlated to the observations (p-value < 0.05) for 15 stations. Among stations with significant statistical scores, the correlation coefficients and the RMSE range from 0.65 to 0.89 and from 0.030 $m^3\,m^{-3}$ to 0.082 $m^3\,m^{-3}$, respectively. The average correlation coefficient and RMSE are 0.77 and 0.053 $m^3\,m^{-3}$, respectively. For most SMOSMANIA stations located in southwestern France, the correlation scores are better than those obtained by Albergel et al. (2011). This is related to the use of LAI and of bipolarized T_b values at a low incidence angle (20°) as additional factors in this study, and to the use of reprocessed SMOS data. Note that for the 11 stations considered by Albergel et al. (2011), fewer observations are available in this study (from 31 to 50, against 44 to 107 in Albergel et al., 2011), because two T_b incidence angles are used.

Also, Table 3 presents the A, B, C, D, E regression coefficient values and the F intercept coefficient obtained in this configuration. They are specific to each site. They may depend on the soil and vegetation properties acting on the microwave emission, like soil roughness, soil surface infiltration and thermal properties, vegetation phenology and canopy structure. For all the stations, the D coefficient, related to the 20 V T_b, is

HESSD
8, 8565–8607, 2011

equal to zero. Therefore, only one term in V polarization plays a role in the regression. Similar results are obtained with different incidence angles (not shown).

3.2.2 Over France

The same regression Eq. (2) with the same configuration (incidence angles of 20° and 40°) as before, was applied using the ISBA-A-gs SSM over France instead of the in situ SSM for the estimation of the correlation coefficients. It produced a spatially distributed SMOS-L1 SSM. Moreover, the correlation between both SMOS-L2 and ASCAT SSM data with the ISBA-A-gs SSM was analyzed over France using Eqs. (3)–(4).

Figure 8 presents the score maps (correlation coefficient r and RMSE) over France of Eqs. (2)–(4). Only significant values (p-value < 0.05) were plotted. The average correlation coefficients over France for SMOS-L1, SMOS-L2, and ASCAT SSM are 0.45, 0.49, and 0.61, respectively. The average RMSE values are $0.075\,m^3\,m^{-3}$, $0.072\,m^3\,m^{-3}$, and 0.75 (dimensionless), respectively. The three SSM estimates correlate better with the ISBA-A-gs SSM in the western part of the country. The West to East decrease in correlation in particularly pronounced for SMOS-L1 and ASCAT. The RMSE follows the same behavior. It was checked that the number of satellite observations used in the regressions does not present this longitudinal contrast and that it has no influence on the obtained spatial patterns of the scores.

The regression coefficients over France for SMOS-L1, SMOS-L2 and ASCAT are presented in Fig. 9. For the SMOS-L1 SSM, derived from T_b values, the B and D coefficients (corresponding to V-polarized T_b) tend to present values closer to zero than the A and C coefficients (corresponding to H-polarized T_b). It must be noted that using Eq. (2) without the LAI factor gives more weight to the 20 V T_b factor. This indicates that the 20 V T_b may be linked with the vegetation opacity. In order to understand the spatial distribution of the coefficients, we searched analogies of their spatial patterns, with the spatial distribution of vegetation types and soil characteristics used by the LSM, and with the precipitation climatology, but no similarity was observed. Moreover, in western France, the E regression coefficient of Eq. (2), relative to LAI, is close to zero while,

HESSD
8, 8565–8607, 2011

on the other hand, LAI information is key in eastern France. The F intercept coefficient presents analogies with the topography (Fig. 1). Low negative values of F correspond to higher altitudes, and four French mountainous regions appear: part of the Pyrenees, Jura, Vosges and Massif Central. Note that most of the Alps area is flagged. The spatial correlation between altitude and F values is $r = -0.51$.

For the SMOS-L2 SSM, a significant spatial correlation between altitude and values of the B' intercept coefficient is observed, also ($r = 0.37$). It is less marked than for the SMOS-L1 F parameter, but data are not provided for the highest mountain ranges such as the Alps and part of the Pyrenees. For ASCAT, no correlation between the altitude and the B^* coefficient is observed ($r = 0.07$). This result shows the impact of topography on the SMOS signal.

4 Discussion

The comparison of SMOS and ASCAT SSM estimates with independent SSM observations and simulations over France in Figs. 3 and 5 shows that, overall, better results are obtained with ASCAT. Apart from the fact that the SMOS-L2 product is still in the evaluation phase, while the ASCAT SSM product exists since 2007 and benefits from the heritage of the ERS SSM product, key physical processes governing the SMOS and ASCAT measurements differ. They are discussed below.

4.1 Impact of the sampling depth

In this study, three soil moisture datasets are considered along with the SMOS-L2 product: the ASCAT SSM, the ISBA-A-gs SSM, and the in situ SMOSMANIA observations at a depth of 5 cm. These different SSM estimates do not present the same sampling depth, and slight differences in sampling depth can affect the temporal variability of SSM in response to rainfall events. As observed by Albergel et al. (2010), the ASCAT SSM product better correlates with LSM simulations representing a skin surface soil

HESSD
8, 8565–8607, 2011

moisture, than with in situ observations at 5 cm. This is not true for the SMOS-L2 SSM, as it present a correlation with LSM simulations similar to its correlation with in situ observations at 5 cm. Indeed, in both cases, the average temporal correlation at the location of the 21 SMOSMANIA stations is equal to 0.36.

4.2 Topography and other geographical factors

The impact of a marked topography can be explained by multiple local incidence angles caused by the different slopes of mountainous areas, affecting the T_b values and, consequently, the SSM retrievals. Mialon et al. (2008) have shown that relief features can cause T_b variations of up to 5 K. Sect. 3.2.2 show that this effect is visible in the SMOS products, both in the SSM derived from the SMOS-L1 data and in the SMOS-L2 data, using the intercept coefficients of Eq. (2) and Eq. (3), F and B', respectively. It must be noted that the fact that F correlates better with topography than B' (r values of −0.51 and 0.37, respectively) could denote an impact of topography on ancillary LAI and T_{eff} information used in Eq. (2).

In order to search for other possible perturbing factors, an analysis of F and B' intercepts was performed. A linear regression between the altitude of each grid-cell (Z) and the intercepts was computed. The same analysis was applied to the ASCAT B^* term. The residual terms of the regressions are shown in Fig. 10. In the three cases, some topography features still appear in the residual term (e.g. the Vosges). This may denote a non-linear impact of Z on SSM retrievals. Moreover, for SMOS-L1, the area corresponding to the eastern SMOSMANIA stations (from Narbonne (NBN) to CBR) presents small scale variations which could denote the presence of RFI.

4.3 Use of the SMOS-L1 product

The results presented in Sect. 3.2.2 show that calibrating statistical relationships based on reference SSM values produced by a LSM permits to produce SSM estimates from the SMOS-L1 product. The scores of the calibrated statistical models are probably the

HESSD
8, 8565–8607, 2011

best achievable scores over France using SMOS data, and the SMOS-L1 SSM outperforms the SMOS-L2 SSM: (1) for the SMOSMANIA in situ observations, the mean temporal absolute correlations of the two SSM estimates are 0.75 and 0.49, respectively, (2) for the LSM simulations over France, the mean temporal correlations of the anomalies of the two SSM estimates are 0.44 and 0.40, respectively. This result shows that Eq. (3) could be used in the assimilation of SMOS-L1 data in LSM. Indeed, SSM observations need to be rescaled to fit the model climatology, before being assimilated (Reichle and Koster, 2004; Draper et al., 2011b), and Eq. (3) could be used during this phase.

4.4 RFI

Table 3 shows that a higher fraction of SMOS-L1 data are affected by RFI for the eastern SMOSMANIA stations (LGC, MZN, VLV, BRN, Méjannes-le-Clap (MJN), BRZ, CBR), with more than 60 % missing data. For MZN, BRN and BRZ, less than 10 observations were available, and the regression model was not applied. Apart from VLV, p-values higher than 0.001 are observed. For the whole SMOSMANIA network, 55 % of the observations had to be removed, on average. In spite of the filtering procedure described in Sect. 2.1.1 and in Sect. 2.4.2, the SMOS data could be affected by undetected low-level RFI.

5 Conclusion

In this study, the first SMOS L1 and L2 products were compared with another satellite soil moisture product, the ASCAT SSM, over France. Independent SSM estimates, derived from either in situ observations in southern France, or LSM simulations over the whole of France, were used to perform a multiple comparison with the satellite products. Although SMOS and ASCAT do not use the same measurement technique, nor the same microwave frequency, consistent results were found, especially in wet

HESSD
8, 8565–8607, 2011

conditions. On the other hand, a number of differences was evidenced. In particular, the soil sampling depth is deeper in the SMOS measurements, and this affected the correlation of the SMOS-L2 product with the skin SSM simulated by the ISBA-A-gs LSM. Also, perturbing geographic spatial patterns such as topography could be extracted from the SMOS-L1 and SMOS-L2 products, and, to a lesser extent, from the ASCAT SSM.

Overall, the ASCAT SSM outperformed the SMOS-L2 product. As the quality of the SMOS products is affected by RFI, this conclusion is valid for the RFI intensity observed in France, and more work is needed to benchmark the SSM products in other areas.

The findings of Albergel et al. (2011) that simple regression equations can be applied across scales on the SMOS-L1 product, was confirmed for the whole of France, in contrasted surface conditions. This method could offer a simple way to ingest SMOS data into LSM using data assimilation techniques.

Acknowledgements. The work of M. Parrens was supported by Université Paul Sabatier, Toulouse. The work of E. Zakharova was supported by the STAE (Sciences et Technologies pour l'Aéronautique et l'Espace) foundation, in the framework of the CYMENT project, and by the "Programme Terre Océan Surface Continentales et Atmosphère" (TOSCA, CNES). The work of S. Lafont, was supported by the GEOLAND2 project, co-funded by the European Commission within the GMES initiative in FP7. W. Wagner acknowledges the support of the Austrian Space Applications Programme (ASAP) and EUMETSAT for the ASCAT data processing.

The publication of this article is financed by CNRS-INSU.

HESSD
8, 8565–8607, 2011

References

Albergel, C., Rüdiger, C., Pellarin, T., Calvet, J.-C., Fritz, N., Froissard, F., Suquia, D., Petitpa, A., Piguet, B., and Martin, E.: From near-surface to root-zone soil moisture using an exponential filter: an assessment of the method based on in-situ observations and model simulations, Hydrol. Earth Syst. Sci., 12, 1323–1337, doi:10.5194/hess-12-1323-2008, 2008.

Albergel, C., Rüdiger, C., Carrer, D., Calvet, J.-C., Fritz, N., Naeimi, V., Bartalis, Z., and Hasenauer, S.: An evaluation of ASCAT surface soil moisture products with in-situ observations in Southwestern France, Hydrol. Earth Syst. Sci., 13, 115–124, doi:10.5194/hess-13-115-2009, 2009.

Albergel, C., Calvet, J.-C., de Rosnay, P., Balsamo, G., Wagner, W., Hasenauer, S., Naeimi, V., Martin, E., Bazile, E., Bouyssel, F., and Mahfouf, J.-F.: Cross-evaluation of modelled and remotely sensed surface soil moisture with in situ data in southwestern France, Hydrol. Earth Syst. Sci., 14, 2177–2191, doi:10.5194/hess-14-2177-2010, 2010.

Albergel, C., Zakharova, E., Calvet, J.-C., Zribi, M., Pardé, M., Wigneron, J.-P., Novello, N., Kerr, Y., Mialon, A., and Fritz, N.: A first assessment of the SMOS data in southwestern France using in situ and airborne soil moisture estimates: the CAROLS airborne campaign, Remote Sens. Environ., 115, 2718–2728, doi:10.1016/j.rse.2011.06.012, 2011.

Attema, E. W. P.: The active microwave instrument onboard the ERS-1 satellite, Proc. IEEE, 79, 791–799, 1991.

Bartalis, Z., Hasenauer, S., Naeimi, V., and Wagner, W.: WARP-NRT 2.0 Reference Manual, ASCAT Soil Moisture Report Series, No. 14, Institute of Photogrammetry and Remote Sensing, Vienna University of Technology, Austria, 26, 2007a.

Bartalis, Z., Wagner, W., Naeimi, V., Hasenauer, S., Scipal, K., Bonekamp, H., Figa, J., and Anderson, C.: Initial soil moisture retrievals from the METOP-A advanced Scatterometer (ASCAT), Geophys. Res. Lett., 34, L20401, doi:10.1029/2007GL031088, 2007b.

Beljaars, A., Viterbo, P., Miller, M., and Betts, A.: The anomalous rainfall over the United States during July 1993: sensitivity to land surface parameterization and soil moisture anomalies, Mon. Weather Rev., 124, 362–383, 1996.

Boone, A. and Etchevers, P.: An inter-comparison of three snow schemes of varying complexity coupled to the same land-surface model: local scale evaluation at an Alpine site, J. Hydrometeorol., 2, 374–394, 2001.

Boone, A., Calvet, J.-C., and Noilhan, J.: Inclusion of a third soil layer in a land surface scheme

HESSD
8, 8565–8607, 2011

using the force-restore method, J. Appl. Meteorol., 38, 1611–1630, 1999.
Brocca, L., Melone, F., Moramarco, T., Wagner, W., and Hasenauer, S.: ASCAT soil wetness index validation through in-situ and modeled soil moisture data in central Italy, Remote Sens. Environ., 114, 2745–2755, 2010b.
Calvet, J.-C., Noilhan, J., Roujean, J.-L., Bessemoulin, P., Cabelguenne, M., Olioso, A., and Wigneron, J.-P.: An interactive vegetation SVAT model tested against data from six contrasting sites, Agr. Forest Meteorol., 92, 73–95, 1998.
Calvet, J.-C., Fritz, N., Froissard, F., Suquia, D., Petitpa, A., and Piguet, B.: In-situ soil moisture observations for the CAL/VAL of SMOS: the SMOSMANIA network, International Geoscience and Remote Sensing Symposium, IGARSS, Barcelona, Spain, 1196–1199, doi:10.1109/IGARSS.2007.4423019, 23–28 July 2007.
Calvet, J.-C., Wigneron, J.-P., Walker, J., Karbou, F., Chanzy, A., and Albergel, C.: Sensitivity of passive microwave observations to soil moisture and vegetation water content: L-band to W-band, IEEE Trans. Geosci. Remote. Sens., 49, 1190–1199, doi:10.1109/TGRS.2010.2050488, 2011.
Chanzy, A., Schmugge, T. J., Calvet, J.-C., Kerr, Y., van Oevelen, P., Grosjean, O., and Wang, J. R.: Airborne microwave radiometry on a semi-arid area during HAPEX-Sahel, J. Hydrology, 188–189, 285–309, 1997.
Cleveland, W. S. and Devlin, S. J.: Locally-Weighted Regression: An approach to regression analysis by local fitting, J. Amer. Statistical Assoc., 83, 596–610, doi:10.2307/2289282, 1988.
Deardorff, J. W.: Efficient prediction of ground surface temperature and moisture with inclusion of a layer of vegetation, J. Geophys. Res., 83, 1889–1903, 1978.
De Wit, A. J. and van Diepen, A. J.: Crop model data assimilation with the ensemble Kalman filter for improving regional crop yield forecasts, Agric. For. Meteorol., 146, 38–56, 2007.
Diermeyer, P. A.: Using a global soil wetness dataset to improve seasonal climate simulation, J. Climate, 13, 2900–2922, 2000.
Dirmeyer, P. A., Dolman, A. J., and Sato, N.: The pilot phase of the global soil wetness project, B. Am. Meteorol. Soc., 80, 851–878, 1999.
Dorigo, W. A., Scipal, K., Parinussa, R. M., Liu, Y. Y., Wagner, W., de Jeu, R. A. M., and Naeimi, V.: Error characterisation of global active and passive microwave soil moisture datasets, Hydrol. Earth Syst. Sci., 14, 2605–2616, doi:10.5194/hess-14-2605-2010, 2010.
Draper, C., Mahfouf, J.-F., Calvet, J.-C., Martin, E., and Wagner, W.: Assimilation of ASCAT

HESSD
8, 8565–8607, 2011

near-surface soil moisture into the French SIM hydrological model, Hydrol. Earth Syst. Sci. Discuss., 8, 5427–5464, doi:10.5194/hessd-8-5427-2011, 2011a.
Draper, C. S., Mahfouf, J.-F., and Walker, J. P.: Root zone soil moisture from the assimilation of screen-level variables and remotely sensed soil moisture, J. Geophys. Res., 116, D02127, doi:10.1029/2010JD013829, 2011b.
Durand, Y., Brun, E., Merindol, L., Guyomarc'h, G., Lesaffre, B., and Martin, E.: A meteorological estimation of relevant parameters for snow models, Ann. Geophys., 18, 65–71, 1993.
Eagleman, J. R. and Lin, W.C.: Remote sensing of soil moisture by a 21-cm passive radiometer. J. Geophys. Res., 81, 3660–3666, 1976.
Eltahir, E. A. B.: A soil moisture rainfall feedback mechanism 1 Theory and observations, Water Resour. Res., 34, 765–776, 1998.
Faroux, S., Roujean, J.-L., Kaptué, A., and Masson, V.: La base de données de paramètres de surface ECOCLIMAP-II sur l'Europe, Note de centre du Groupe de Météorologie à Moyenne Echelle, 86, Météo-France, CNRM, Toulouse, France, 120 pp., 2009.
Fennessy, M. J. and Shukla, J.: Impact of initial soil wetness on seasonal atmospheric prediction, J. Climate, 12, 3167–3180, 1999.
Georgakakos, K. P. and Carpenter, M.: Potential value of operationally available and spatially distributed ensemble soil water estimates for agriculture, J. Hydrol., 328, 177–191, 2006.
Guerif, M. and Duke, C. I.: Adjustment procedures of a crop model to the site-specific characteristics of soil and crop using remote sensing data assimilation, Agric. Ecosyst. Environ., 81, 57–69, 2000.
Jackson, T. J.: Profile soil moisture from space measurements, J. Irr. Drain. Div.-ASCE, 106, 81–92, 1980.
Jackson, T., Le Vine, D., Swift, C., Schmugge, T., and Schiebe, F.: Large area mapping of soil moisture using the ESTAR passive microwave radiometer in Washita92, Remote Sens. Environ., 53, 27–37, 1995.
Jackson, T. J., Hsu, A. Y., van de Griend, A., and Eagleman, J. R.: Skylab L band microwave radiometer observations of soil moisture revisited, Int. J. Remote Sens., 25, 2585–2606, 2004.
Kerr, Y.: Soil moisture from space: Where are we?, Hydrogeology Journal, 15, 117–120, 2007.
Kerr, Y.: SMOS level 2 Processor for Soil Moisture, Algorithm Theoretical Basis Document (ATBD), 133 pp., 2010.
Kerr, Y. H. and Njoku, E. G.: On the use of passive microwave at 37 GHz in remote sensing of

HESSD
8, 8565–8607, 2011

vegetation, Int. J. Remote Sens., 14, 1931–1943, 1993.
Kerr, Y., Waldteufel, P., Wigneron, J.-P., Martinuzzi, J.-M., Font, J., and Berger, M.: Soil Moisture retrieval from space: the Soil Moisture and Ocean Salinity (SMOS) mission, IEEE T. Geosci. Remote, 39, 1729–1736, 2001.
Ledoux, E., Girard, G., De Marsily, G., and Deschenes, J.: Spatially distributed modeling: Conceptual approach, coupling surface water and ground-water, in: Unsaturated Flow Hydrologic Modeling: Theory and Practice, NATO ASI Series C, vol. 275, edited by: Morel-Seytoux, H. J., 435–454, Kluwer Acad., Norwell, Mass., 1989.
Le Moigne, P.: SURFEX scientific documentation. Note de centre du Groupe de Météorologie à Moyenne Echelle, 87, Météo-France, CNRM, Toulouse, France, 211 pp., available online at: http://www.cnrm.meteo.fr/surfex/ (last access: September 2011), 2009.
Masson, V., Champeaux, J. L., Chauvin, F., Meriguet, C., and Lacaze, R.: A global database of land surface parameters at 1 km resolution in meteorological and climate models, J. Climate, 16, 1261–1282, 2003.
Mattar, C., Wigneron, J.-P., Sobrino, J. A., Novello, N., Calvet, J.-C., Albergel, C., Richaume, P., Mialon, A., Guyon, D., Jiménez-Muñoz, J. C., and Kerr, Y.: A combined optical-microwave method to retrieve soil moisture over vegetated areas, IEEE Trans. Geosci. Remote. Sens., submitted, 2011.
McMullan, K. D., Martin-Neira, M., Hahne, A., and Borges, A.: SMOS-Earth's Water Monitoring Mission, Space Technologies for the Benefit of Human Society and Earth, Part I, 2009.
Mialon, A., Coret, L., Kerr, Y., Sécherre, F., and Wigneron, J.-P.: Flagging the topographic impact on the SMOS signal, IEEE Trans. Geosci. Remote. Sens., 46, 689–694, 2008.
Njoku, E. G., Ashcroft, P., Chan, T. K., and Li, L.: Global survey and statistics of radiofrenquency interference in AMSR-E land observation, IEEE Trans. Geosci. Remote. Sens., 43, 938–947, 2005.
Noilhan, J. and Mahfouf, J.-F.: The ISBA land surface parameterisation scheme, Global Planet. Change, 13, 145–149, 1996.
Noilhan, J. and Planton, S.: A simple parameterisation of land surface processes for meteorological model, Mon. Weather Rev., 117, 356–549, 1989.
Oliva, R., Daganzo, E., Kerr, Y., Mecklenburg, S., Nieto, S., Richaume, P., and Gruhier, C.: SMOS radio frequency interference scenario: status and actions taken to improve the RFI environment in the 1400–1427 MHz passive band, IEEE Trans. Geosc. Remote Sens., submitted, 2011.

HESSD
8, 8565–8607, 2011

Panciera, R., Walker, J. P., Kalma, J. D., Kim, E. J., Saleh, K., and Wigneron, J.-P.: Evaluation of the SMOS L-MEB passive microwave soil moisture retrieval algorithm, Remote Sens. Environ., 113, 435–444, 2009.

Pardé, T., Zribi, M., Fanise, P., and Dechambre, M.: Analysis of RFI issue using the CAROLS L-band experiment, IEEE Trans. Geosci. Remote Sens., 49, 1063–1070, 2011.

Pellarin, T., Calvet, J.-C., and Wigneron, J.-P.: Surface soil moisture retrieval from L-band radiometry: a global regression study, IEEE Trans. Geosci. Remote Sens., 41, 2037–2051, 2003a.

Pellarin, T., Wigneron, J.-P., Calvet, J.-C., Berger, M., Douville, H., Ferrazzoli, P., Kerr, Y. H., Lopez-Baeza, E., Pulliainen, J., Simmonds, L. P., and Waldteufel, P.: Two-year global simulation of L-band brightness temperatures over land, IEEE Trans. Geosc. Remote Sens., 41, 2135–2139, 2003b.

Pellarin, T., Wigneron, J.-P., Calvet, J.-C., and Waldteufel, P.: Global soil moisture retrieval from a synthetic L-band brightness temperature data set, J. Geophys. Res., 108, 4364, doi:10.1029/2002JD003086, 2003c.

Raju, S., Chanzy, A., Wigneron, J.-P., Calvet, J.-C., Kerr, Y., and Laguerre, L.: Soil moisture and temperature profile effects on microwave emission at low frequencies, Remote Sens. Environ., 54, 85–97, 1995.

Reichle, R. and Koster, R.: Bias reduction in short records of satellite soil moisture, Geophys. Res. Lett., 31, L19501, doi:10.1029/2004GL020938, 2004.

Robock, A., Vinnikov, K. Y., Srinivasan, J. K., Entin, J. K., Hollinger, S. E., Sperenskaya, N. A., Liu, S., and Namkhai, A.: The global soil moisture data bank, B. Am. Meteorol. Soc., 81, 1281–1299, 2000.

Rüdiger, C., Hancock, G., Hemakumara, H. M., Jacobs, B., Kalma, J. D., Martinez, C., Thyer, M., Walker, J. P., Wells, T., and Willgoose, G. R.: Goulburn River experimental catchment data set, Water Resour. Res., 43, 1–10, W10403, doi:10.1029/2006WR005837, 2007.

Rüdiger, C., Calvet, J.-C., Gruhier, C., Holmes, T., De Jeu, R., and Wagner, W.: An intercomparison of ERS-Scat and AMSR-E soil moisture observations with model simulations over France, J. Hydrometeorol., 10, 431–447, doi:10.1175/2008jhm997.1, 2009.

Saleh, K., Wigneron, J.-P., Calvet, J.-C., Lopez-Baeza, E., Ferrazzoli, P., Berger, M., Wursteisen, P., Simmonds, L., and Miller, J.: The EuroSTARRS airborne campaign in support of the SMOS mission: First results over land surfaces, Int. J. Remote Sens., 25, 177–194, 2004.

HESSD

8, 8565–8607, 2011

Saleh, K., Wigneron, J.-P., de Rosnay, P., Calvet, J.-C., Escorihuela, M. J., Kerr, Y., and Waldteufel, P.: Impact of rain interception by vegetation and mulch on the L-band emission of natural grass, Remote Sens. Environ., 101, 127–139, 2006a.

Saleh, K., Wigneron, J.-P., de Rosnay, P., Calvet, J.-C., and Kerr, Y.: Semi-empirical regressions at L-band applied to surface soil moisture retrieval over grass, Remote Sens. Environ., 101, 415–426, 2006b.

Schmugge, T. J.: Remote Sensing of Soil Moisture: Recent Advances, IEEE Trans. Geosci. Remote Sens., GE21, 145–146, 1983.

Schmugge, T. J.: Applications of passive microwave observations of surface soil moisture, J. Hydrol., 212–213, 188–197, 1998.

Scipal, K., Holmes, T., de Jeu, R., Naeimi, V., and Wagner, W.: A possible solution for the problem of estimating the error structure of global soil moisture data sets, Geophys. Res. Lett., 35, L24403, doi:10.1029/2008gl035599, 2008b

Skou, N.: Microwave radiometer systems: design and analysis, MA, Norwood, USA, Artech House, 1989.

Stoffelen, A.: Toward the true near-surface wind speed: Error modeling and calibration using triple collocation, J. Geophys. Res., 103, 7755–7766, doi:10.1029/97jc03180, 1998.

Ulaby, F. T., Moore, R. K., and Fung, A. K.: Physical mechanisms and empirical models for scattering and emission, in: Microwave Remote Sensing: Active and Passive (vol. II), Artech House, Boston, MA, USA, 816–921, 1982.

Ulabay, F., Moore, R., and Fung, A.: Microwave Remote Sensing: Active and Passive, From Theory to Application. Norwwod, MA: Artech House, 1986.

Wagner, W., Lemoine, G., Borgeaud, M., and Rott, H.: A study of vegetation cover effects on ERS scatterometer data, Geosci. Remote Sens., 37, 938–948, 1999a.

Wagner, W., Lemoine, G., and Rott, H.: A method for estimating soil moisture from ERS scatterometer and soil data, Remote Sens. Environ., 70, 191–207, 1999b.

Wagner, W., Noll, J., Borgeaud, M., and Rott, H.: Monitoring soil moisture over the Canadian prairies with the ERS scatterometer, IEEE Trans. Geosci. Remote Sens., 37, 206–216, 1999c.

Wagner, W., Blöschl, G., Pampaloni, P., Calvet, J.-C., Bizzarri, B., Wigneron, J.-P., and Kerr, Y.: Operational readiness of microwave remote sensing of soil moisture for hydrologic applications, Nordic Hydrology, 38, 1–20, 2007.

Wigneron, J.-P., Chanzy, A., Calvet, J.-C., and Bruguier, N.: A simple algorithm to retrieve soil

HESSD

8, 8565–8607, 2011

moisture and vegetation biomass using passive microwave measurements over crop fields, Remote Sens. Environ., 51, 331–341, 1995.
Wigneron, J.-P., Guyon, D., Calvet, J.-C., Courrier, G., and Bruguier, N.: Monitoring coniferous forest characteristics using a multifrequency (5–90 GHz) microwave radiometer, Remote Sens. Environ., 60, 299–310, 1997.
Wigneron, J.-P., Calvet, J.-C., Pellarin, T., Van de Griend, A., Berger, M., and Ferrazzoli, P.: Retrieving near surface soil moisture from microwave radiometric observations: Current status and future plans, Remote Sens. Environ., 85, 489–506, 2003.
Wigneron. J.-P., Calvet, J.-C., de Rosnay, P., Kerr, Y., Waldteufel, P., Saleh, K., Escorihuela, M.-J., and Kruszewski, A.: Soil moisture retrievals from biangular L-band passive microwave observations, IEEE Trans. Geosci. Remote Sens., 1, 277–281, 2004.
Wigneron, J.-P., Kerr, Y., Waldteufel, P., Saleh, K., Escorihuela, M.-J., Richaume, P., Ferrazzoli, P., de Rosnay, P., Gurney, R., Calvet, J.-C, Grant, J.P., Guglielmetti, M., Hornbuckle, B., Mätzler, C., Pellarin, T., and Schwank, M.: L-band Microwave Emission of the Biosphere (L-MEB) Model: Description and calibration against experimental data sets over crop fields, Remote Sens. Environ., 107, 639–655, 2007.
Wigneron, J.-P., Chanzy, A., de Rosnay, P., Rüdiger, C., and Calvet, J.-C.: Estimating the effective soil temperature at L-band as a function of soil Properties, IEEE Trans. Geosc. Remote Sens., 46, 797–807, 2008.
Wilson, W. J., Yuech, S. H., Dinardo, S. J., Chazanoff, S. L., Kitiyakara, A., Li, F. K., and Rahmat-Samii, Y.: Passive active L-band and S-band (PALS) microwave sensor for ocean salinity and soil moisture measurements, IEEE Trans. Geosc. Remote Sens., 39, 1039–1048, 2001.
Zribi, M., Pardé, M., Boutin, J., Fanise, P., Hauser, D., Dechambre, M., Kerr, Y., Leduc-Leballeur, M., Skou, M., Søbjærg, S.S., Albergel, C., Calvet, J.-C., Wigneron, J.-P., Lopez-Baeza, E., Ruis, A., and Tenerelli, J.: CAROLS: a new airborne L-band radiometer for ocean surface and land observations, Sensors, 11, 719–742, doi:10.3390/s110100719, 2011.

HESSD
8, 8565–8607, 2011

Table 1. Soil characteristics of the nine new stations of the SMOSMANIA network at four depths (5, 10, 20 and 30 cm): fractions of clay, sand fraction, organic matter, and bulk density. The station are listed from East to West (Pezenas to Cabrières d'Avignon).

Stations	Depth (cm)	Clay ($g\,kg^{-1}$)	Sand ($g\,kg^{-1}$)	Organic matter ($g\,kg^{-1}$)	Bulk density ($kg\,m^{-3}$)
Pézenas (PZN)					
	5	175	506	49.5	1238
	10	174	519	23.2	1311
	20	161	598	10.9	1266
	30	194	520	11.5	1363
Prades-le-Lez (PRD)					
	5	311	270	54.9	1358
	10	328	237	49.7	1317
	20	323	238	39.8	1409
	30	335	217	35.3	1570
La Grand Combe (LGC)					
	5	129	732	29.7	1536
	10	129	748	21.8	1496
	20	88	815	30.1	1507
	30	139	740	24.1	1507
Mazan-Abbaye (MZN)					
	5	150	676	102	961
	10	126	720	78.2	1330
	20	129	696	68.7	1127
	30	109	664	53.5	1257
Villevieille (VLV)					
	5	136	657	53.4	1116
	10	124	678	26.9	1274
	20	106	695	12.7	1419
	30	118	671	14.9	1381
Barnas (BRN)					
	5	95	773	70.8	1427
	10	71	804	59.8	1630
	20	61	802	30.5	1310
	30	112	767	22.4	1527
Méjannes-le-Clap (MJN)					
	5	162	455	121	1276
	10	193	428	110	1276
	20	257	347	106	1276
	30	202	303	78.1	1276
Berzème (BRZ)					
	5	233	375	38.0	1094
	10	264	346	32.6	1280
	20	257	386	25.9	1394
	30	264	340	25.7	1294
Cabrières d'Avignon (CBR)					
	5	242	476	44.9	1300
	10	233	488	26.3	1310
	20	216	561	23.1	1325
	30	223	498	20.1	1353

HESSD
8, 8565–8607, 2011

Table 2. Comparison of SMOS-L2 and ASCAT SSM anomalies with the in-situ SSM (−5 cm) anomaly measured at 21 ground stations for the year 2010: correlation (r_{ano}), mean bias (in-situ minus satellite products), root mean square error (RMSE) and p-value. The number of data used to calculate the scores is given (n_{ano}). Absolute correlations (r_{abs}) are indicated. NS stands for non significant, and *, **, *** stand for p-values greater than 0.05, between 0.05 and 0.001, and between 0.001 and 0.0001, respectively.

	SMOS-L2								ASCAT							
	Absolute correlations			Anomalies					Absolute correlations			Anomalies				
Stations	n_{abs}	r_{abs}	P-value	n_{ano}	r_{ano}	RMSE	Bias	P-value	n_{abs}	r_{abs}	P-value	n_{ano}	r_{ano}	RMSE	Bias	P-value
SBR	6	0.06	NS	5	0.69	0.81	−0.41	NS	158	0.82	***	153	0.74	0.68	0.05	***
URG	122	0.61	***	116	0.32	1.08	0.06	**	149	0.75	***	139	0.65	0.71	−0.06	***
CRD	119	0.55	***	113	0.27	1.25	0.06	**	165	0.77	***	153	0.53	0.96	0.01	***
PRG	134	0.53	***	127	0.23	1.20	0.03	*	153	0.77	***	143	0.51	0.90	−0.07	***
CDM	131	0.42	***	126	0.25	1.17	0.05	**	164	0.71	***	152	0.63	0.80	−0.02	***
LHS	133	0.47	***	128	0.29	1.11	−0.15	**	152	0.63	***	140	0.45	0.91	−0.10	***
SVN	130	0.48	***	123	0.39	1.06	−0.01	***	154	0.61	***	142	0.45	0.91	−0.11	***
MNT	118	0.39	***	116	0.48	0.91	−0.03	***	151	0.64	***	141	0.52	0.88	−0.07	***
SFL	135	0.42	***	129	0.38	1.00	0.02	***	155	0.58	***	143	0.38	0.97	−0.04	***
MTM	102	0.34	**	97	0.20	1.13	0.11	NS	149	0.14	NS	140	0.12	1.15	−0.05	NS
LZC	23	0.59	**	17	0.60	0.83	0.03	*	33	0.92	***	23	0.96	0.33	0.08	***
NBN	118	0.53	***	113	0.34	1.13	0.05	**	152	0.65	***	142	0.37	1.07	0.05	***
PZN	116	0.52	***	112	0.36	1.01	−0.03	***	167	0.76	***	160	0.58	0.80	−0.07	***
PRD	79	0.54	***	69	0.39	1.02	0.03	**	142	0.42	***	137	0.46	1.00	−0.01	***
LGC	39	0.35	*	26	0.17	1.14	−0.06	NS	143	0.62	***	137	0.65	0.82	−0.04	***
MZN	40	0.48	**	36	0.38	1.01	0.05	*	120	0.19	*	114	0.35	0.98	−0.03	***
VLV	95	0.61	***	90	0.30	1.07	0.14	**	162	0.52	***	155	0.70	1.01	−0.08	***
BRN	12	0.44	NS	8	0.33	1.02	0.19	NS	64	0.58	***	58	0.55	0.91	0.10	***
MJN	55	0.40	**	46	0.36	0.99	−0.04	*	134	0.68	***	126	0.70	0.77	−0.11	***
BRZ	47	0.53	***	40	0.44	1.06	0.19	**	135	0.57	***	132	0.69	0.81	0.02	***
CBR	74	0.51	***	70	0.41	0.92	0.12	**	167	0.46	***	157	0.44	0.97	0.11	***

HESSD
8, 8565–8607, 2011

Table 3. Comparison between the in situ SSM and the SSM retrieved from the SMOS-L1 T_b using the regression coefficients (A, B, C, D, E, F) of Eq. (2) derived from the in situ SSM: number of points used in the regression (n), correlation coefficient (r_{abs}), root mean square error (RMSE) and p-value. The fraction of missing data caused by the RFI filtering is indicated. NS stands for non significant, and *, **, *** stand for p-values greater than 0.05, between 0.05 and 0.001, and between 0.001 and 0.0001, respectively.

Stations	n	r_{abs}	RMSE($m^3\,m^{-3}$)	p-value	A	B	C	D	E	F	Altitude (m)	% of missing data
SBR	–	–	–	–	–	–	–	–	–	–	74	–
URG	37	0.88	0.054	***	0.6645	0.0567	0.0816	0	−0.1050	0.9251	135	39
CRD	43	0.82	0.030	***	0.4343	0.0752	0.1428	0	−0.0971	−0.2683	149	36
PRG	43	0.72	0.043	***	0.4427	0.1198	−0.0624	0	−0.0675	−0.2289	183	33
CDM	40	0.74	0.048	***	0.1862	0.1101	0.2234	0	−0.0171	0.0706	118	34
LHS	35	0.67	0.064	***	0.2776	0.0631	0.1676	0	−0.0237	−0.0684	207	35
SVN	33	0.83	0.069	***	0.2985	0.0012	0.3377	0	−0.0918	0.6340	122	39
MNT	42	0.73	0.066	***	0.5533	0.0704	0.2049	0	0.0680	0.5692	255	35
SFL	39	0.79	0.043	***	0.5107	0.0083	0.1568	0	−0.0066	0.0053	236	39
MTM	26	0.77	0.032	***	0.2608	−0.0344	0.1580	0	−0.0095	−0.6162	499	31
LZC	–	–	–	–	–	–	–	–	–	–	102	–
NBN	43	0.81	0.039	***	1.3620	−0.0218	0.2924	0	−0.1013	0.6836	33	33
PZN	38	0.69	0.057	***	2.4201	0.1508	−0.0991	0	−0.0864	1.3057	39	30
PRD	16	0.89	0.049	***	−0.7565	0.8619	−0.0251	0	−0.2245	−0.8958	99	40
LGC	13	0.49	0.034	NS	0.9649	0.3521	−0.5398	0	−0.0883	−0.2759	436	63
MZN	–	–	–	–	–	–	–	–	–	–	1165	–
VLV	22	0.86	0.055	***	1.6293	0.1919	0.1118	0	−0.2052	2.2735	51	83
BRN	–	–	–	–	–	–	–	–	–	–	672	–
MJN	10	0.75	0.082	*	0.3015	0.2545	−0.1205	0	−0.1796	0.1262	268	69
BRZ	–	–	–	–	–	–	–	–	–	–	540	–
CBR	13	0.65	0.069	*	1.0116	0.9940	0.0994	0	0.1113	1.1543	584	68

HESSD
8, 8565–8607, 2011

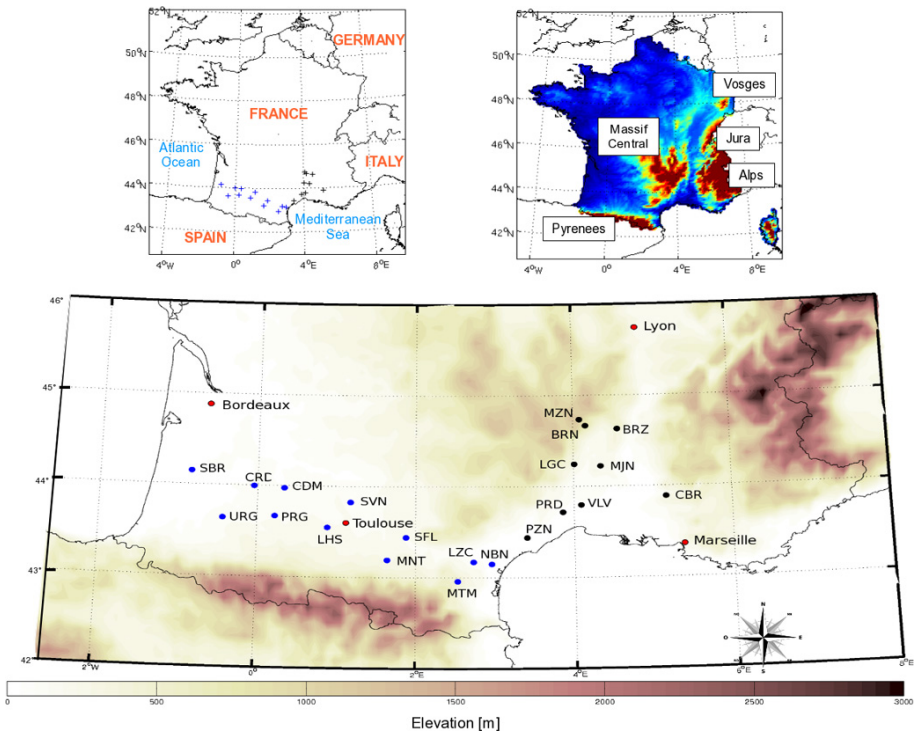

Fig. 1. The SMOSMANIA soil moisture network in southern France. The blue dots and crosses represent the 12 stations operational since 2007, the dark dots and crosses represent the new 9 stations operational since 2009. Topography is shown (bottom, top-right) together with the main mountainous areas (top-right).

HESSD
8, 8565–8607, 2011

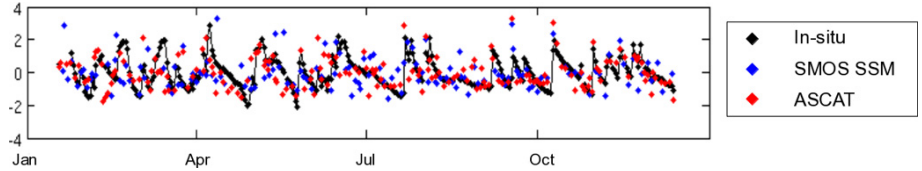

Fig. 2. Observed SSM anomalies at the Montaut (MNT) station in 2010, derived from (black) in situ measurements at a 5cm depth, (blue) SMOS-L2, (red) ASCAT.

HESSD
8, 8565–8607, 2011

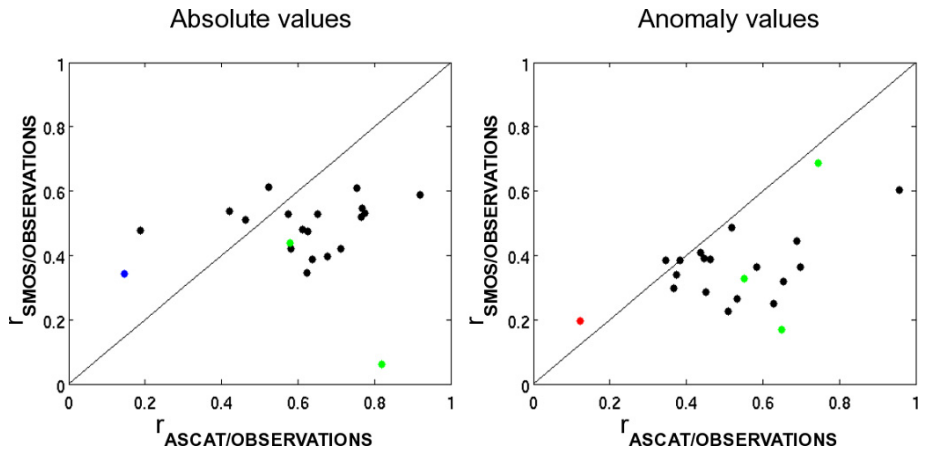

Fig. 3. SMOS-L2 vs. ASCAT SSM (left) absolute and (right) anomaly correlation coefficients with the SMOSMANIA in situ observations for each SMOSMANIA station. Black dots represent significant SSM correlations for both SMOS and ASCAT. Green dots represent significant SSM correlations for ASCAT, only. The blue dot indicates a significant SSM correlation for SMOS, only. The red dot corresponds to the MTM station, presenting no significant correlation (p-value > 0.05) for either SMOS or ASCAT.

HESSD
8, 8565–8607, 2011

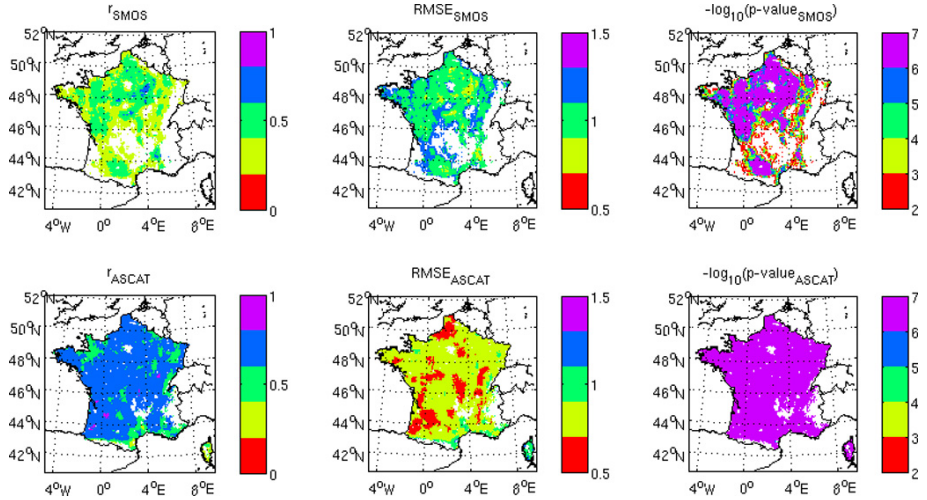

Fig. 4. Comparison between SMOS-L2 and ASCAT SSM anomalies with SSM anomalies calculated by ISBA-A-gs. From left to right: correlation coefficient (r), root mean square error (RMSE), and p-value, for (top) SMOS-L2, and (bottom) ASCAT. Blanked areas are mountainous or urban areas and areas presenting a non-significant score (p-value > 0.05).

HESSD
8, 8565–8607, 2011

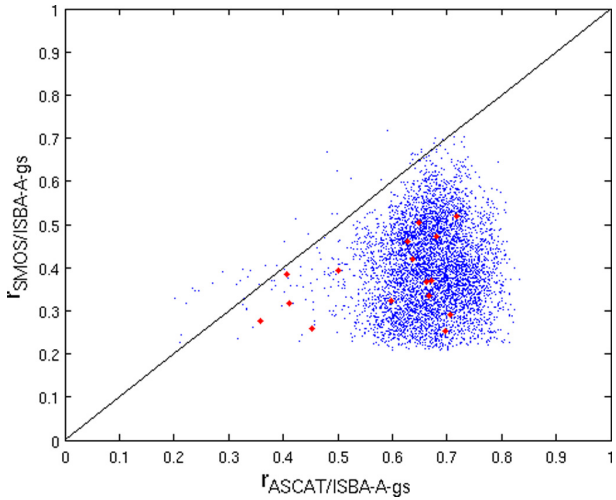

Fig. 5. SMOS-L2 vs. ASCAT SSM anomaly correlation coefficients with the ISBA-A-gs simulations for each ISBA-A-gs grid cell. Red dots represent the ISBA-A-gs grid-cells corresponding to SMOSMANIA stations. Only points presenting significant correlations (p-value < 0.05) for both SMOS-L2 and ASCAT are shown.

HESSD
8, 8565–8607, 2011

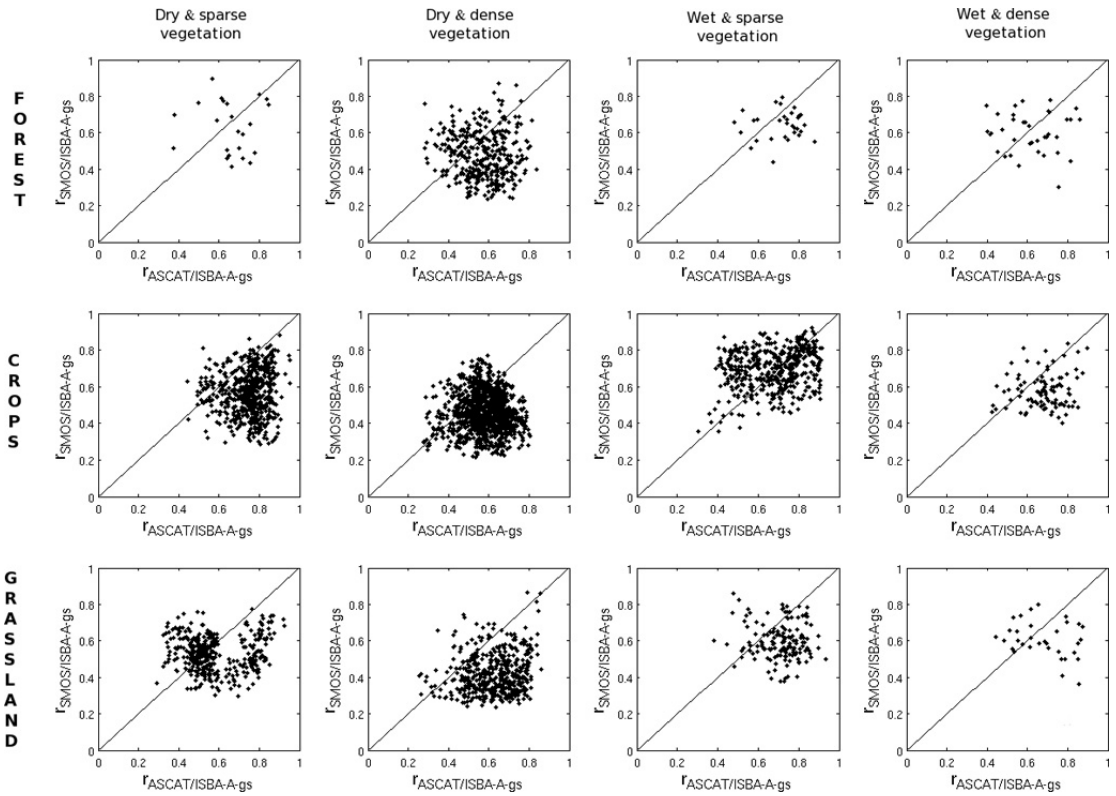

Fig. 6. Impact of vegetation density (dense and sparse) and soil wetness conditions (wet and dry) on SMOS-L2 vs. ASCAT SSM anomaly correlation coefficients with the ISBA-A-gs simulations for crops, forests, and grasslands.

HESSD
8, 8565–8607, 2011

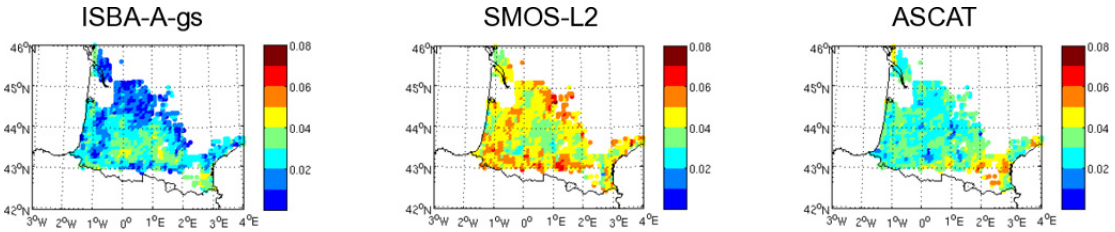

Fig. 7. Relative error estimation for SMOS-L2, ASCAT and ISBA-A-gs SSM anomalies derived from a triple collocation analysis. The errors are expressed in units of $m^3\,m^3$.

HESSD
8, 8565–8607, 2011

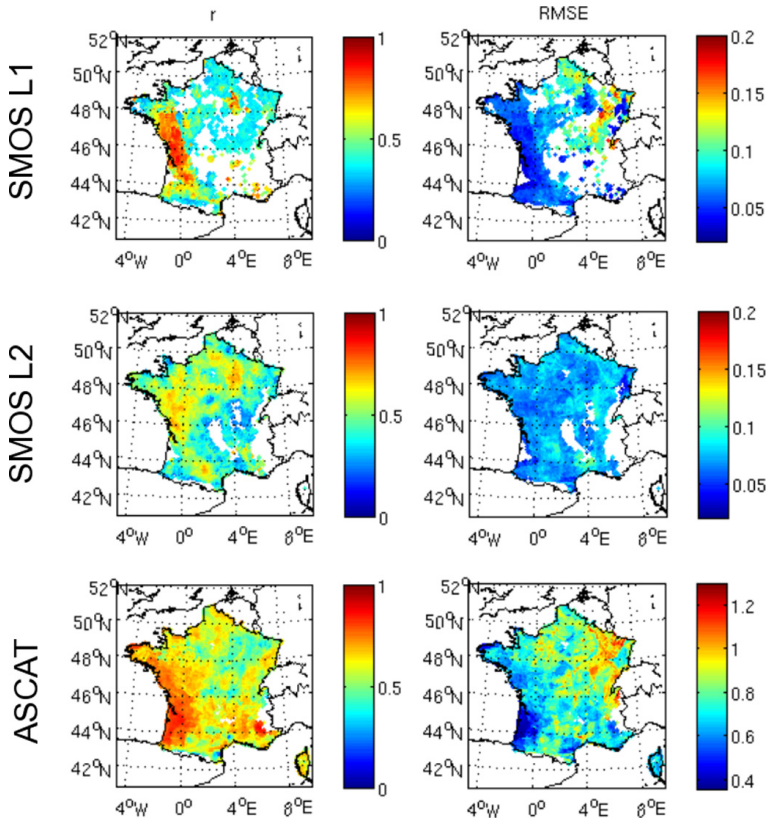

Fig. 8. Regression statistics of satellite vs. ISBA-A-gs SSM in 2010: (left) correlation coefficient (r) and (right) root mean square error (RMSE), of (top) SMOS-L1 with Eq. (2), (middle) SMOS-L2 with Eq. (3), (bottom) ASCAT with Eq. (4). The RMSE is expressed in $m^3\ m^{-3}$ in the dynamic range of ISBA-A-gs for SMOS, and in dimensionless units for ASCAT.

HESSD
8, 8565–8607, 2011

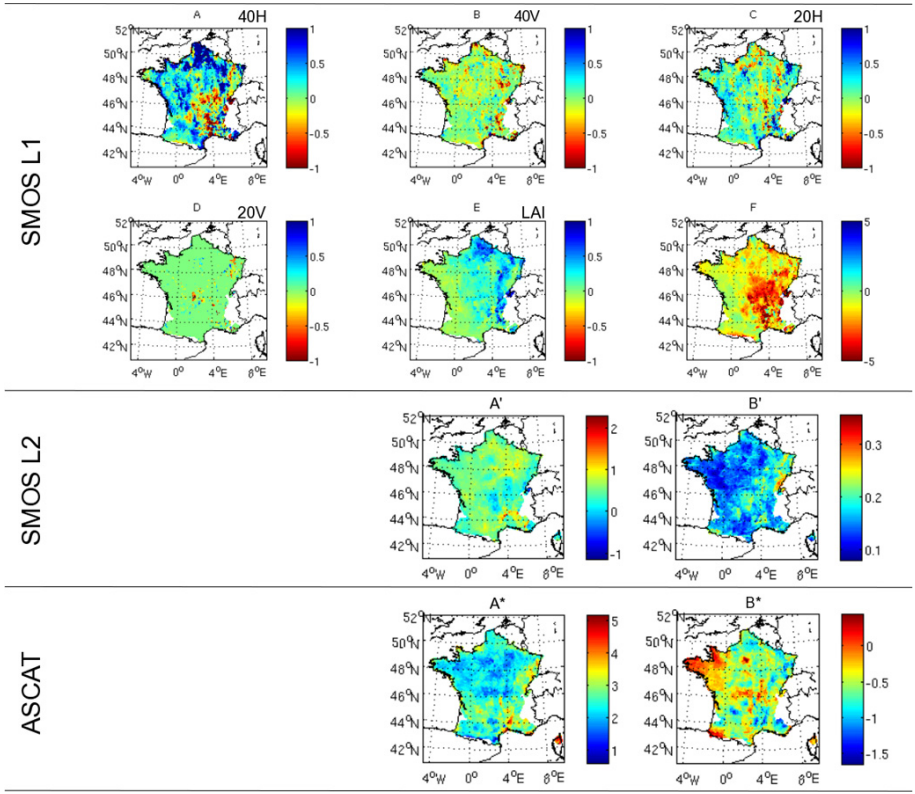

Fig. 9. Regression coefficients of satellite vs. ISBA-A-gs SSM in 2010: (top) SMOS-L1 with Eq. (2), (middle) SMOS-L2 with Eq. (3), (bottom) ASCAT with Eq. (4).

HESSD
8, 8565–8607, 2011

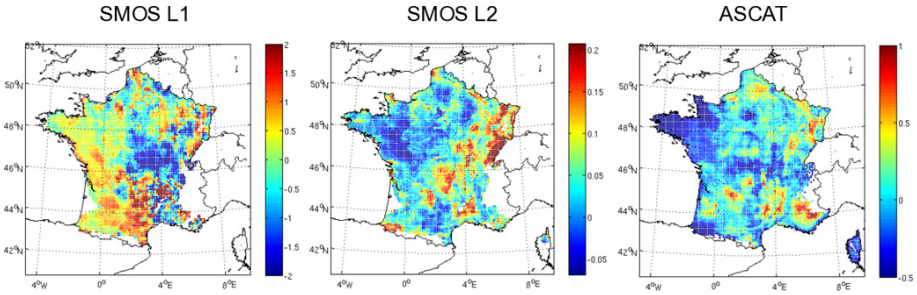

Fig. 10. Residual term of the regression equation of (left) SMOS-L1 F, (centre) SMOS-L2 B', (right) B^* intercepts vs. altitude (Z).

HESSD
8, 8565–8607, 2011